



UNIVERSITY OF LEEDS

This is a repository copy of *Astrochemical Significance of the P + SO Reaction: Spectroscopic Characterization of SPO, PSO and SOP isomers*.

White Rose Research Online URL for this paper:
<https://eprints.whiterose.ac.uk/170178/>

Version: Accepted Version

Article:

Trabelsi, T, Plane, JMC orcid.org/0000-0003-3648-6893 and Francisco, JS (2021) Astrochemical Significance of the P + SO Reaction: Spectroscopic Characterization of SPO, PSO and SOP isomers. *Astrophysical Journal*, 909 (2). 122. ISSN 0004-637X

<https://doi.org/10.3847/1538-4357/abdd3c>

© 2021. The American Astronomical Society. All rights reserved. This is an author-created, un-copyedited version of an article published in *Astrophysical Journal*. IOP Publishing Ltd is not responsible for any errors or omissions in this version of the manuscript or any version derived from it. The Version of Record is available online at <https://doi.org/10.3847/1538-4357/abdd3c>

Reuse

Items deposited in White Rose Research Online are protected by copyright, with all rights reserved unless indicated otherwise. They may be downloaded and/or printed for private study, or other acts as permitted by national copyright laws. The publisher or other rights holders may allow further reproduction and re-use of the full text version. This is indicated by the licence information on the White Rose Research Online record for the item.

Takedown

If you consider content in White Rose Research Online to be in breach of UK law, please notify us by emailing eprints@whiterose.ac.uk including the URL of the record and the reason for the withdrawal request.



eprints@whiterose.ac.uk
<https://eprints.whiterose.ac.uk/>

Astrochemical Significance of the P + SO Reaction: Spectroscopic Characterization of SPO, PSO and SOP isomers.

Tarek Trabelsi¹, John M. C. Plane² and Joseph S. Francisco¹

¹ Department of Earth and Environmental Science and Department of Chemistry, University of Pennsylvania, Philadelphia, PA, USA 19104-6316

² School of Chemistry, University of Leeds, Leeds, LS2 9JT, U.K.

E-mail: frjoseph@sas.upenn.edu

Received xxxxxx

Accepted for publication xxxxxx

Published xxxxxx

Abstract

The doublet and quartet potential energy surfaces for the P + SO → PO + S reaction are explored using the highly accurate explicit correlation multireference configuration interaction method, and the reaction is found to be thermodynamically favourable, with an exothermicity value of 70.5 kJ/mol. The electronic structure, spectra, and bond dissociation energies of the intermediates involved in the reaction, such as SPO, PSO and SOP, are calculated using high-level quantum chemistry methods. An explanation of the non-detection of the diatomic SP is proposed. At pressures relevant to astrochemistry, the reaction is overwhelmingly bimolecular, with a predicted rate coefficient of $2.1 \times 10^{-10} (T/300)^{-0.23} \text{ cm}^3 \text{ molecule}^{-1} \text{ s}^{-1}$. The results from this study are expected to aid in the spectroscopic detection of these new species in the laboratory and the interstellar medium.

Keywords: PES, SPO, phosphorus monoxide, rate coefficient.

1. Introduction

Phosphorus plays an essential chemical role in life on Earth. It is fundamental to all living things and is an important nutrient for animals and plants. It plays a critical role in cell development and is a key component of molecules that store energy, such as ATP (adenosine triphosphate), DNA and lipids (fats and oils). Thus, phosphorus is an essential element for life and may be linked to the origin of life on Earth and play a role as a marker for life on temperate exoplanets (Griffith et al. 1977; Gulick 1957; Maciá et al. 1997). However, the origin of phosphorus on early Earth is a mystery.

The observation that phosphorus is found in Comet 67P/C-G strengthens the link between comets and life on Earth (Altwegg et al. 2016).

Phosphorus-bearing molecules have been detected in diatomic form, such as PO, PN and CP, in the circumstellar envelopes of AGB stars (Lefloch et al. 2016; Milam et al. 2008; Tenenbaum et al. 2007; Turner & Bally 1987; Yamaguchi et al. 2011); and triatomic and tetratomic forms, such as C₂P (Halfen et al. 2008), HCP (Agúndez et al. 2007) and PH₃ (Agúndez et al. 2014). Their formation is still poorly understood. For instance, the observed PO abundance in the inner wind of IKTau was found to be ~3 orders of magnitude

larger than that simulated by a comprehensive chemical network (Gobrecht et al. 2016). Depending on the temperature and radius of the envelope, many plausible mechanisms have been proposed to explain the formation of phosphorus-bearing molecules. On the one hand, diatomic species such as CP, PO, PN and PH may be products of triatomic parent species such as HCP, i.e., $\text{HCP} + h\nu \rightarrow \text{H} + \text{CP}$ (Namai et al. 2009), or another phosphorus-bearing parent molecule, such as PNO or HPO. In this case, the photodissociation mechanism may explain the formation of the diatomic species, and the known electronic spectroscopy properties of the parent molecules provide important insight into this mechanism. On the other hand, diatomic species can also form through shock or reactive collisions (Jiménez-Serra et al. 2018) such as



or



In these cases, some intermediates may play an important role in the formation of diatomic species, such as in the case of reaction (2). It should be noted that the gas-phase chemistry in oxygen-rich circumstellar shells suggests that a reaction with PN could lead to the formation of PNO or its isomers. Both the shock reaction and the photodissociation mechanism of phosphorus-bearing molecules suffer from a lack of both theoretical and experimental investigations. For instance, the rates of reactions (1) and (2) have been estimated from the fact that N and P are isovalent, but the reactions have not been measured or theoretically calculated.

Sulfur monoxide (SO) is an important diatomic agent in the interstellar medium (ISM) due to its relative elemental abundance relative to that of other species and its role as a key intermediate in the oxidation of elemental sulfur (De Beck et al. 2013; Rivilla et al. 2016; Tenenbaum et al. 2007). With abundances of 10^5 cm^{-3} at 90 km in Earth's atmosphere (Gómez Martín et al. 2017) it is important to Earth's sulfur chemical cycle above the stratosphere. Due to the importance of SO, the triatomic [S, P, O] molecular system may play significant role. Atom + diatom reactions such as



may compete with other reactions (1) and (2) to explain the formation of the diatomic PO.

PO and SO have been detected in several regions in the ISM. However, no experimental or theoretical studies on the triatomic SPO molecular system have yet been performed.

In this study, we use high accuracy *ab initio* methods, such as coupled cluster theory, to spectroscopically characterize the electronic ground states of the SPO, SOP and PSO isomers.

These species may play an important role in reaction (3). This data is crucial for the detection of these species, both in the laboratory and in the ISM. We then explore the electronic potential energy surfaces connecting the reactants, intermediates and products in order to use Rice-Ramsperger-Kassel-Markus (RRKM) theory (Gilbert and Smith, 1990) to calculate the rate coefficient of reaction 3, which may be an important source of PO in the ISM.

2. Methods

Electronic structure calculations of all the SPO isomers were performed using coupled cluster CCSD(T) (Knowles et al. 1993, 2000) and explicitly coupled cluster CCSD(T)-F12 (Knizia et al. 2009) theory. Considering the small multireference character of the SPO isomers, the complete active space self-consistent field (CASSCF) (Knowles & Werner 1985; Werner & Knowles 1985) and internally contracted multireference MRCI (Knowles & Werner 1988; Werner & Knowles 1988) methods were also used sequentially. For a more accurate description of the electron correlation, the MRCI-F12 and Davidson correction MRCI+Q methods were used (Szalay & Bartlett 1993). In these calculations, the aug-cc-pV(X+d)Z (X=D, T, Q and 5) basis sets (Dunning Jr 1989; Dunning Jr et al. 2001; Wilson et al. 1996) were used for CCSD(T), and the cc-pVnZ-F12 (X=D, T and Q) basis sets (Peterson et al. 2008) were used for CCSD(T)-F12. Additional calculations using the core-consistent aug-cc-pWCVXZ-DK (X=D, T and Q) basis set (Jorge et al. 2009) including all electrons, i.e., CCSD(T)(A.E.), were performed to consider the core-valence and relativistic effect correction. The total energies and geometrical parameters in the present calculations were therefore extrapolated to the CBS limit for each basis set family using the two-parameter equations $\text{EX} = \text{ECBS} + \text{A}/\text{X}^3$, where A is a fitting parameter. The three-dimensional potential energy surfaces (3D-PESs) were mapped in the corresponding internal coordinates (RSP, RSO, RPO and θ) and calculated at the CCSD(T)(A.E.)/aug-cc-pWCVQZ-DK level. These calculations were performed at several nuclear geometries around the respective equilibrium geometry, and a set of spectroscopic parameters were generated using the SURFIT (Senekowitsch 1988) program.

3. Results and discussion

3.1 Spectroscopy, stability and chemical insights

The relative energies, rotational constants and equilibrium geometries of all SPO isomers are listed in **Table 1**. Only the ground state of each isomer was considered. The

reactions between SO and P, between SP and O and between PO and S generated four isomers. The most stable isomer was the bent SPO with predicted SP and PO bond lengths of 1.9153 Å and 1.4723 Å, respectively, at the CCSD(T)/CBS level of theory. Inclusion of the core-valence and relativistic effects at the CCSD(T)(A.E.)/CBS level led to shortening of the bonds, predicting SP and PO bond lengths of 1.9084 Å and 1.4673 Å, respectively. Explicit treatment of the electron correlation at the MRCI-F12 level of theory predicted SP and PO bond lengths in agreement with those calculated at the CCSD(T) level of theory, whereas the calculations using Davidson correction at MRCI+Q poorly described the SP and PO distances, which were predicted to be 0.0208 Å and 0.0144 Å larger than those calculated at the CCSD(T)/CBS level. The effect of this difference can be easily seen in the rotational constants. For instance, the difference was larger than 3500 MHz for the A_e constant. In further discussions, we will quote and recommend the equilibrium geometries calculated at the CCSD(T)(A.E.)/CBS level of theory. The second isomer, *cyc-SPO*(X^2A''), lay at 1.62 eV above the global minimum at all CCSD(T)/CBS levels of theory. This value is consistent with the MRCI-F12 level and 0.1 eV lower than those calculated at the CCSD(T) level. For the equilibrium geometry, the MRCI+Q values were larger than those calculated at the MRCI-F12 or CCSD(T) level. It should be noted that the *cyc-SPO* isomer can be considered an excited state of SPO since they have different state symmetries. There are 6 electronic doublet states, $^2A''$ (3) and $^2A'$ (3), in the C_s symmetry group that correlate to the first dissociation limits of SO+P, PS+O or PO+S, and *cyc-SPO* may have formed through the reaction of atom + diatom.

The PSO isomer was predicted to be bent like SPO and to lie at 1.88 eV above the SPO isomer. Again, the MRCI+Q level of theory poorly predicted the equilibrium geometries of the PSO isomer. For example, the SP bond length and the

bending angle were predicted to be 0.0451 Å and 1.2° larger than those calculated at the CCSD(T)(A.E.)/CBS level of theory. Explicit treatment of the electron correlation at the MRCI-F12 level of theory gave results in good agreement with the CCSD(T) results. At the CCSD(T)(A.E.)/CBS level of theory, the SP and SO bond lengths were predicted to be 1.9724 Å and 1.4765 Å, respectively. At the same level of theory, the SP bond length was 0.064 Å larger than that predicted in the SPO isomer.

The SOP isomer lay at 3.01 eV above the global minimum, with a predicted bending angle of 135.5° at the CCSD(T) level of theory. This result is inconsistent with those calculated at the MRCI level of theory. The rotational constants calculated using multireference and single-reference methods are not consistent, especially when we compare the rotational constants. For instance, the rotational constants A_e showed a difference of ~22000 MHz, which may be due to the difference in the bending angles. In comparison, the PO distance increased by 0.1747 Å relative to its value in the SPO isomer at CCSD(T)(A.E.)/CBS level of theory. This comparison suggests a small bond dissociation energy along the P-OS bond length compared to that of SPO. Moreover, both SO and PO were increased in the SOP isomer relative to their values in free diatomic SO ($X^3\Sigma^-$, $r_e=1.4810$ Å) and PO ($X^2\Pi$, $r_e=1.4759$ Å).

SPO (X^2A')							
Method/basis set	SP	PO	θ	A_e	B_e	C_e	E_r
CCSD(T)/CBS	1.9153	1.4723	133.0	68070	4377	4110	0.0
CCSD(T)-F12/CBS	1.9142	1.4718	133.0	68280	4385	4124	0.0
CCSD(T)(A.E.)/CBS	1.9084	1.4673	133.0	68329	4400	4131	0.0
MRCI+Q/aug-cc-pV(T+d)Z	1.9361	1.4867	132.1	64580	4323	4051	0.0
MRCI-F12/aug-cc-pVTZ	1.9093	1.4749	132.9	67847	4406	4137	0.0
Recommended	1.9084	1.4673	133.0	68329	4400	4131	0.0
<i>cyc-SPO</i> (X^2A'')							
	SO	PO	θ	A_e	B_e	C_e	E_r
CCSD(T)/CBS	1.7730	1.6538	73.6	21195	7553	5568	1.62
CCSD(T)-F12/CBS	1.7723	1.6455	73.6	21233	7569	5579	1.62
CCSD(T)(A.E.)/CBS	1.7798	1.6464	73.5	21020	7452	5501	1.62
MRCI+Q/aug-cc-pV(T+d)Z	1.7936	1.6629	73.6	20909	7415	5474	1.52
MRCI-F12/aug-cc-pVTZ	1.7811	1.6507	73.7	21228	7512	5548	1.66
Recommended	1.7798	1.6464	73.5	21020	7452	5501	1.62
PSO (X^2A')							

	SP	SO	θ	A_e	B_e	C_e	E_r
CCSD(T)/CBS	1.9811	1.4797	118.4	40368	4720	4226	1.87
CCSD(T)-F12/CBS	1.9763	1.5014	118.5	40586	4727	4234	1.87
CCSD(T)(A.E.)/CBS	1.9724	1.4765	118.5	40557	4740	4244	1.88
MRCI+Q/aug-cc-pV(T+d)Z	2.0175	1.4974	117.3	38209	4617	4119	1.78
MRCI-F12/aug-cc-pVTZ	1.9864	1.4851	118.5	40287	4696	4206	1.89
Recommended	1.9724	1.4765	118.5	40557	4740	4244	1.88
SOP(X^2A')							
	PO	SO	θ	A_e	B_e	C_e	E_r
CCSD(T)/CBS	1.5986	1.6439	135.2	103952	3560	3442	3.01
CCSD(T)-F12/CBS	1.5948	1.6418	135.3	104021	3566	3447	2.99
CCSD(T)(A.E.)/CBS	1.5940	1.6420	135.3	103923	3571	3452	3.01
MRCI+Q/aug-cc-pV(T+d)Z	1.6264	1.6549	129.7	81719	3633	3478	2.73
MRCI-F12/aug-cc-pVTZ	1.6183	1.6400	129.9	83380	3679	3524	2.92
Recommended	1.6183	1.6400	129.9	83380	3679	3524	2.92

Table 1: Equilibrium geometries (distances in Å and angles in degrees), rotational constants (in MHz), and relative energies (in eV) of the SPO, *cyc*-SPO, PSO and SOP isomers.

To aid in the detection of SPO isomers, a set of accurate spectroscopic constants were determined from the 3D-PESs calculated at the CCSD(T)(A.E.)/aug-cc-pWCVQZ-DK level of theory. These parameters included equilibrium bond distances (r_e), rotational constants at the equilibrium geometry (A_e , B_e , and C_e), first-order centrifugal distortion constants (D_j), vibrational anharmonicity constants (χ_{ij}), dipole moment and anharmonic (ν_i) and harmonic (ω_i) vibrational frequencies, and they are reported in **Table 2**.

The vibrational frequencies of SPO and PSO suggest that the ro-vibrational spectra are further complicated because of the existence of anharmonic resonances (e.g., the Darling-Dennison and Fermi resonances). For instance, the symmetric mode of the SPO isomer, which was predicted to be 609 cm^{-1} , is two times the asymmetric mode i.e. $2\nu_3 = \nu_1$. This is expected to result in Fermi resonances. For the PSO isomer, we observed the same trend, where the asymmetric mode was predicted to be 1082 cm^{-1} and the symmetric mode was predicted to be 556 cm^{-1} . In the SOP isomer, the bending mode was predicted to be 132 cm^{-1} , consistent with the other levels of theory, which all predicted a value less than 150 cm^{-1} . This small bending mode suggests that the potential energy surface along the bending mode will be flat, and a large amplitude of motion is expected. This conclusion is also supported by the observation that the DK distortion constant is significantly larger than other quartic distortion constants. This latter value was predicted to be 176.5 cm^{-1} for SOP and 2.8 cm^{-1} for PSO. Moreover, the small value of the bending mode can be probed using far-IR sources either in the laboratory or at synchrotron radiation sources. **Table 2** shows that the asymmetric frequency modes are characterized by bright intensities,

suggesting that their detection through vibrational spectroscopy is likely. For instance,

	SPO(X^2A')	PSO(X^2A')	SOP(X^2A')
R_{SP} (Å)	1.9107	1.9778	
R_{SO} (Å)		1.4787	1.6445
R_{PO} (Å)	1.4695		1.5969
θ (°)	134.0	118.4	135.0
A_e (MHz)	71266	40638	103283
B_e (MHz)	4386	4740	3578
C_e (MHz)	4132	4244	3458
D_j (MHz)	0.0013	0.0024	0.0029
D_{jk} (MHz)	-0.1007	-0.0716	-1.2248
D_k (MHz)	9.9459	2.8374	176.56
μ_e (D)	0.60	0.90	0.63
χ_{11} (cm^{-1})	-9.205	-9.461	-34.838
χ_{22} (cm^{-1})	-20.628	-0.772	-1.422
χ_{33} (cm^{-1})	-13.853	-0.991	-3.177
χ_{12} (cm^{-1})	-2.449	-3.062	-10.009
χ_{13} (cm^{-1})	-20.104	-8.766	4.085
χ_{23} (cm^{-1})	-12.354	2.536	4.002
ω_1 (cm^{-1})	1233	1107	909
ω_2 (cm^{-1})	332	242	138
ω_3 (cm^{-1})	641	561	604
ν_1 (cm^{-1})	1203(252)	1082(1000)	836(260)
ν_2 (cm^{-1})	325(15)	240(15)	132(1)
ν_3 (cm^{-1})	609(58)	556(18)	602(22)
$2\nu_2$	637	479	262
$\nu_2 + \nu_3$	947	799	738
$3\nu_2$	936	716	388
$2\nu_3$	1191	1110	1198
$2\nu_2 + \nu_3$	1271	1040	872
$2\nu_1$	2389	2146	1603

Table 2: CCSD(T)(A.E.)/aug-cc-pWCVQZ-DK spectroscopic constants of SPO, PSO and SOP isomers in their ground electronic states. The values in parentheses are the MP2/aug-cc-pV(T+d)Z intensities.

the intensity of the ν_1 mode for PSO is predicted to be 1000 km/mol, which would greatly facilitate its detection. The asymmetric ν_1 mode for the SPO and SOP isomers shows relatively high intensities of 252 and 260 km/mol.

3.2 Formation of PO through SO + P and SP + O reactions and photochemistry of the intermediate complexes

Despite the detection of PO and SO in VY CMa stars and the relatively high abundance of sulfur and oxygen in the same region, no isomers of the [S, P, O] molecular system have been detected. In the gas phase or on grain surfaces, SPO isomers may form through SO + P, SP + O and PO + S reactions. These reactions may generate SPO species in their excited or ground electronic states.

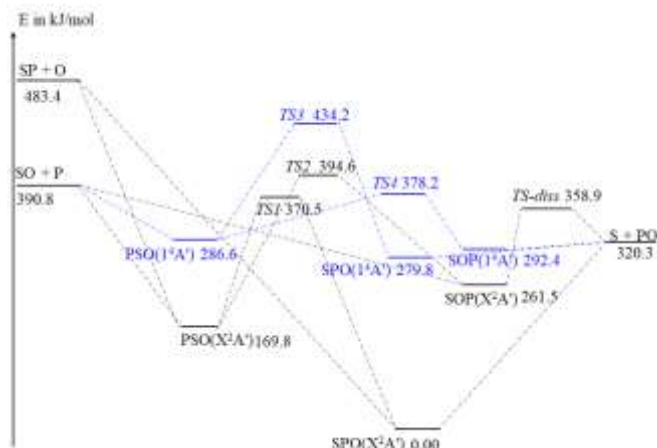
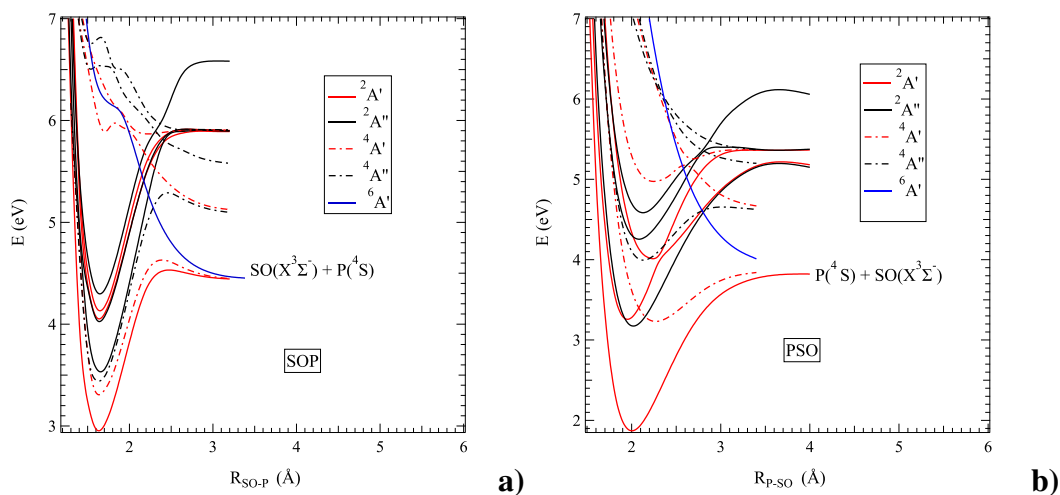


Figure 1: Doublet (black) and quartet (blue) potential energy surfaces for the [S, P, O] system calculated at the MRCI+Q/aug-cc-pV(T+d)Z level of theory, including the lowest dissociation limits. The transition states are single-point calculations at their optimized equilibrium geometries at the CASSCF/aug-cc-pV(T+d)Z level. The dissociation limits were calculated at the CCSD(T)(A.E.)/aug-cc-pWCVQZ-DK level.

The bond dissociation energies (BDEs) of all SPO isomers were calculated at the CCSD(T)(A.E.)/aug-cc-pWCVQZ-DK level of theory and are shown in **Figure 1**. The correlation of the lowest doublet and quartet electronic states to the SO+P and PO+S dissociation limits is shown in **Figure 2**.



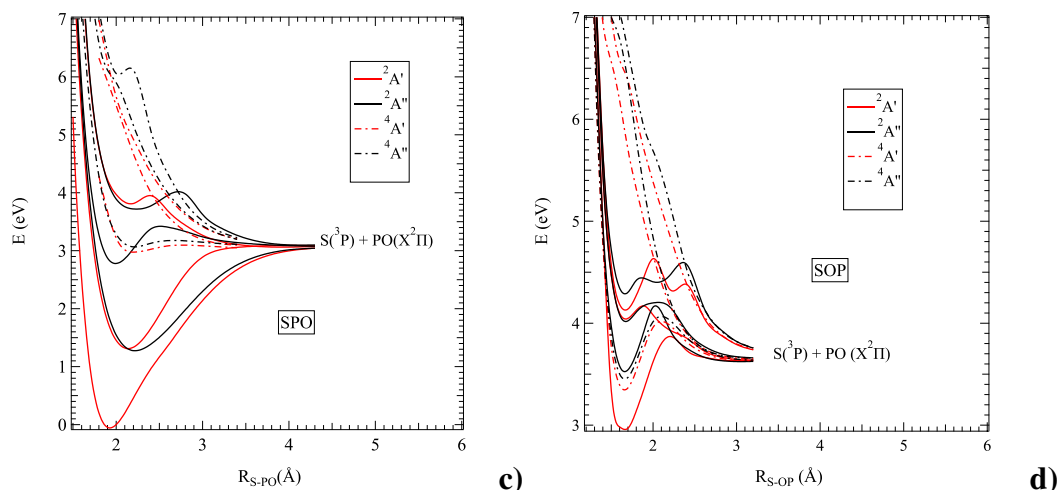


Figure 2: MRCI+Q/aug-cc-pV(Q+d)Z PESs along the stretching and bending coordinates. **a)** and **d)** for SOP along the PO and SO distances, respectively. **b)** for PSO along the PS distance. **c)** for SPO along the SP distance.

The vertical excitation energies are listed in **Table 3**. Inspection of these values shows that the formation of PO via the SO + P reaction is plausible from a thermodynamic perspective. The SO + P \rightarrow PO + S reaction is exothermic, with a predicted exothermicity of 0.73 eV (70.41 kJ/mol).

This reaction occurs adiabatically in a single doublet electronic state (**Figure 2a and 2b**). This reaction involves the SOP isomer when the phosphorus atom attacks the oxygen in the diatomic SO (**Figure 2a**).

Transition	SPO		PSO		SOP		cyc-SPO		
	λ (nm)	f	λ (nm)	f	λ (nm)	f	Transition	λ (nm)	f
$2^2A' \leftarrow X^2A'$	724.8	0.0052	812.1	0.0065	1143.7	0.0020	$1^2A' \leftarrow X^2A''$	3190.5	0.0004
$3^2A' \leftarrow X^2A'$	293.1	0.0324	578.7	0.0043	1068.3	0.0040	$2^2A' \leftarrow X^2A''$	2257.8	0.0018
$1^2A'' \leftarrow X^2A'$	672.6	0.0196	973.2	0.0009	2129.5	0.0002	$3^2A' \leftarrow X^2A''$	1034.4	0.0001
$2^2A'' \leftarrow X^2A'$	432.7	0.0144	531.9	0.0034	1169.6	0.0008	$2^2A'' \leftarrow X^2A''$	439.1	0.0026
$3^2A'' \leftarrow X^2A'$	298.8	0.0059	466.9	0.0018	933.1	0.0004	$3^2A'' \leftarrow X^2A''$	243.0	0.0071

Table 3: MRCI+Q/aug-cc-pV(Q+D)Z vertical excitation energy (λ in nm) and the oscillator strength of each transition f .

This isomer is characterized by a small S-OP BDE of 0.33 eV (31.8 kJ/mol) and an S-OP BDE of 1.06 eV (102.2 kJ/mol). The production of PO may occur through the upper vibrational levels of the ground-state X^2A' . The reaction of SO and P may also lead to the formation of the PSO isomer when the phosphorus atom attacks the sulfur of the SO (**Figure 2b**).

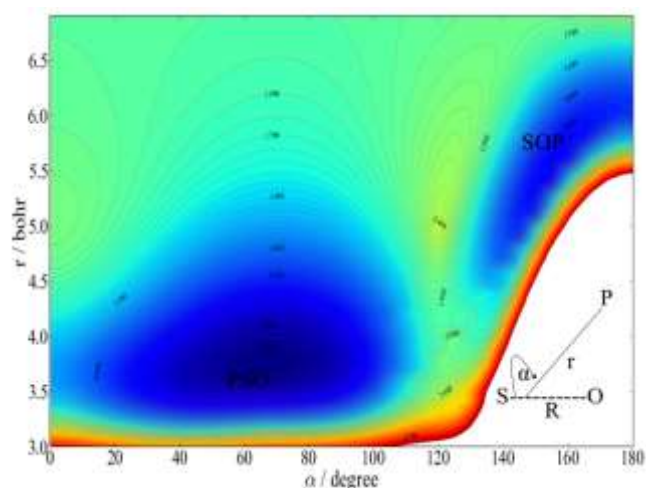


Figure 3: MRCI+Q/aug-cc-pV(T+d)Z two-dimensional PES in eV for the motion of the phosphorus atom around the diatomic SO.

Figure 3 shows the evolution of the ground state of SOP and PSO along the Jacobi coordinates (r, α). In the SOP and PSO isomers, the SO distance does not change much and was kept fixed at its equilibrium values in SOP during the calculations of the PES (**Figure 3**). This figure shows that the transition state that connects SOP and PSO is located at ~ 2.4 eV (240 kJ/mol) above the global minimum (named TS2 in **Figure 1**). Inspection of this figure also shows that the reaction of S and PO favours SOP and SPO with a linear configuration in the entrance channel. Indeed, over a long range, i.e., $r=6.5$ bohr and $\alpha < 160^\circ$, there is a high barrier that prevents the formation of PSO. This barrier decreases as SO and P adopt a linear configuration, i.e., $170 < \alpha < 180^\circ$.

The reaction of SP with oxygen may lead to formation of the SPO isomer when the oxygen atom attacks the phosphorus of diatomic SP (**Figure 2c**). Moreover, the electronic ground state of SPO correlates to the first dissociation limit of PO + S, and the SPO isomer may be involved in the formation of PO. In this case, other processes are in competition with this process, for example, photodissociation, since the S-PO BDE was calculated to be 3.32 eV (320.3 kJ/mol) for the SPO isomer. The MRCI/aug-cc-pV(Q+d)Z vertical excitation energy of the $3^2A' \leftarrow X^2A'$ electronic transition was predicted to be 293.1 nm with a relatively large transition dipole moment (0.61 D) and oscillator strength (0.0324). Absorption into this state may produce diatomic PO since the $3^2A'$ state is unstable and has a minimum located above the first dissociation limit of S+PO (see **Figure 2c**). All SPO isomers show a high density of electronic states in the ultraviolet visible (UV-Vis) region, which favours their crossing and spin-orbit coupling.

The inverse reaction, PO+S, may lead to formation of the SPO isomer when the oxygen atom attacks the phosphorus of diatomic PO from the sulfur side. **Figure 2c** shows that the potential energy surface of the ground state correlates adiabatically to the PO+S dissociation limit, and there is no barrier to prevent this reaction. Attack of the phosphorus atom leads to SOP, and this reaction needs to overcome a small energy barrier (denoted as TS-diss in **Figure 1**) of 0.4 eV (38.6 kJ/mol).

Thus, there are two plausible mechanisms for the formation of the diatomic PO: (i) an attack of the SO diatomic by atomic phosphorus followed by cleavage the SO bond and formation of PO; (ii) the formation of SPO or PSO isomers and their photodissociation to produce PO and S.

In the long range, the doublet and quartet states cross mutually, and the formation of SPO isomers may occur in the

quartet state. **Figure 2a** and **2b** shows that the $1^4A'$ state is stable and shows a minimum below the first dissociation limit. This state correlates adiabatically to the first dissociation limit of SO + P. In the PSO isomer, the BDE for SO + P was predicted to be 104.2 kJ/mol, and that for PO + S was predicted to be 27.9 kJ/mol. The transition states that connect the quartet minima were also calculated and named TS3 and TS4 in **Figure 1**. Compared to that on the doublet surface, the conversion from PSO to SPO or SOP on the quartet surface requires less energy. For instance, conversion from PSO to SOP requires 224.6 kJ/mol on the doublet surface, while it requires only 91.6 kJ/mol on the quartet surface.

3.3 Lack of the SP diatomic

The study of chemical reactions involving SO and PO has been very limited, and the processes studied here are potentially important in understanding the formation and destruction of PO in space and may also explain the non-detection of diatomic SP. **Figure 1** shows that the SP + O dissociation limit is high in energy and makes the reactions that produce SP from SO or PO endothermic. Moreover, reactions that involve SPN (Trabelsi et al. 2018), HPS, and H₂PS (Lopez et al. 1993) as intermediates to produce diatomic SP may occur in the ISM, but they are also endothermic. Quantitative analyses of the reaction $SX + P \rightarrow SP + X$ ($X = N, O, H_2$ and H) allow us to suggest that the non-detection of the diatomic SP may be explained by the fact that the dissociation limits of SP + X ($X = N, O, H_2$ and H) are high in energy and that all reactions that may produce SP are endothermic. This suggests that the diatomic SP, if it exists, should be generated in high temperature regions, where shocks allow strongly endothermic chemistry to occur.

3.4 Kinetics of the P + SO \rightarrow PO + S Reaction

Collisions between P(4S) and SO($^3\Sigma^-$) take place on PESs of A' symmetry and doublet, quartet and sextet spin multiplicity. However, the sextet surfaces are repulsive and do not contribute to the reaction. The doublet and quartet surfaces each split into two pathways, as illustrated in **Figure 1**. All four pathways to the bimolecular products PO($^2\Pi$) + S(3P) are either barrierless (the quartet surface via SOP) or involve barriers that are submerged with respect to the reactants (the doublet surface via PSO and SPO, the double surface via SOP, and the quartet surface via PSO and SOP). To model this complex scenario, RRKM calculations were performed using the Master Equation Solver for Multi-Energy well Reactions (MESMER) program (Glowacki et al. 2012). The internal energy of each species on the PESs was divided into a contiguous set of grains (width 200 cm⁻¹) containing a bundle

of rovibrational states. The rotational constants and vibrational frequencies required to calculate the densities of all the stationary points on the PESs in **Figure 1** are listed in **Table 4**.

	R _{SP}	R _{SO}	R _{PO}	θ	A	B	C	ω ₁	ω ₂	ω ₃	ZPVE
⁴ SPO	2.2097		1.5145	120.9	40347	3824	3493	1072	192	325	795
⁴ PSO	2.2142	1.5241		102.0	25638	4548	3863	987	199	424	805
⁴ SOP		1.6651	1.6929	113.4	46736	4068	3742	813	194	813	838
TS1	1.9377	1.7913		63.2	13453	3110	2526	694	491	i432	593
TS2		1.6285	1.9917	75.3	20365	6338	4833	844	269	i265	557
TS3	1.9626		2.3044	80.7	10607	6022	3841	648	157	i377	622
TS4	2.1650	1.6559		63.26	19403	6051	4613	814	439	i674	402
TS-diss		2.8584	1.5040	123.6	55586	2333	2239	1005	156	i110	580

Table 4 : Equilibrium geometries (distances in Å and angles in degrees), rotational constants (in MHz), harmonic vibrational frequencies and zero-point vibrational energies (ZPVEs) (in cm⁻¹).

Each grain was then assigned a set of microcanonical rate coefficients, for dissociation either back to P + SO or forward to PO + S where appropriate, using an inverse Laplace transformation to link them directly to the relevant high-pressure limiting recombination coefficient ($k_{\text{rec},\infty}$). $k_{\text{rec},\infty}$ was set to the capture rate calculated using the long-range transition state method of Klippenstein and Georgievskii (Georgievskii & Klippenstein 2005), which yields $k_{\text{rec},\infty}(\text{P} + \text{SO}) = 6.8 \times 10^{-10} (T/300)^{1/6} \text{ cm}^3 \text{ molecule}^{-1} \text{ s}^{-1}$ and $k_{\text{rec},\infty}(\text{PO} + \text{S}) = 7.0 \times 10^{-10} (T/300)^{1/6} \text{ cm}^3 \text{ molecule}^{-1} \text{ s}^{-1}$. In both cases, the dispersion force dominates capture.

For P + SO, 1/3 of collisions statistically take place on the ²A' surface, which splits into 2 pathways, so the $k_{\text{rec},\infty}$ for each reaction pathway was set to 1/6 of $k_{\text{rec},\infty}(\text{P} + \text{SO})$, i.e., $1.1 \times 10^{-10} (T/300)^{1/6} \text{ cm}^3 \text{ molecule}^{-1} \text{ s}^{-1}$. The same applies for the two pathways arising from the ⁴A' surface. Collisions between PO and S generate three A' surfaces of doublet spin multiplicity and three A' surfaces of quartet spin multiplicity. There are three additional ²A'' and three ⁴A'' surfaces, but these do not correlate with the reactants. Each A' surface therefore has a statistical weight of 1/12, so the $k_{\text{rec},\infty}$ for each surface was set to $5.8 \times 10^{-11} (T/300)^{1/6} \text{ cm}^3 \text{ molecule}^{-1} \text{ s}^{-1}$. The standard RRKM transition state treatment (Georgievskii & Klippenstein 2005; Gilbert & Smith 1990; Glowacki et al. 2012) was used to calculate the microcanonical rate coefficients for crossing the saddle points between the local minima in **Figure 1**. The probability of collisional transfer between grains was calculated using the exponential down model, taking H₂ as the third body because of the astrochemical environment. The average energy for downward transitions $\langle \Delta E \rangle_{\text{down}}$ was set to 200 cm⁻¹ at 300 K,

with a small temperature dependence of $T^{0.25}$ (Gilbert & Smith 1990).

Figure 4 illustrates the calculated rate coefficient for the total removal of P as a function of [H₂] at 300 and 1000 K, as well as the rate coefficients of the individual reaction channels. The bimolecular reaction to PO + S dominates over recombination at pressures up to approximately 10 bar at 300 K and more than 1000 bar at 1000 K. There are two doublet surfaces that lead to PO + S via ²SOP and ²SPO. The former is faster because it has a lower submerged barrier, but this pathway is still slower than the reaction via ⁴SOP, which has no barriers. The most important recombination products are ²PSO and then ⁴PSO because these local minima are reasonably deep and occur before substantial barriers on their respective surfaces. ²SOP and ⁴SOP are less important, and the latter is weakly bound and will quickly dissociate into PO + S.

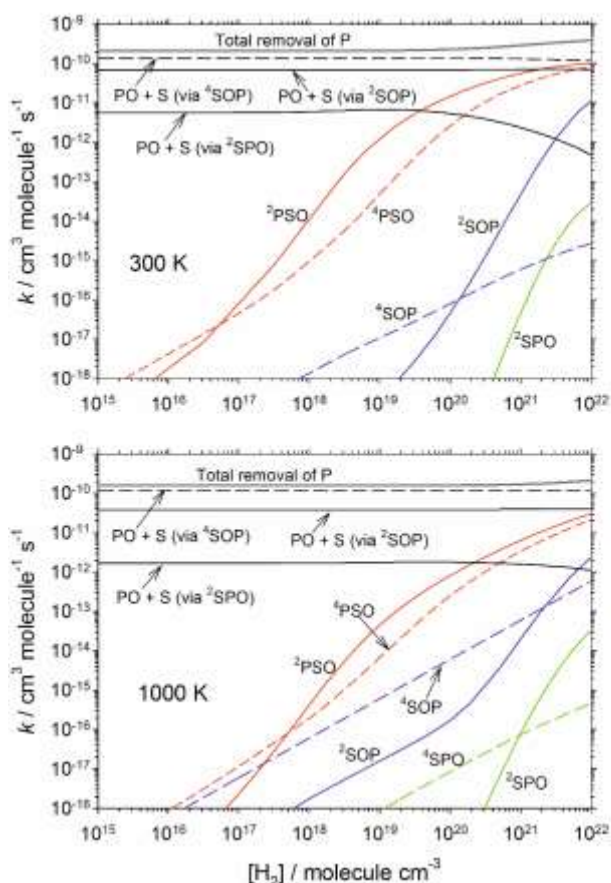


Figure 4. Rate coefficients as a function of the H_2 bath gas concentration for the reaction between P and SO at 300 K (top panel) and 1000 K (bottom panel). The thick grey line is the total P removal reaction rate coefficient. This comprises three bimolecular pathways to PO + S (black lines) and recombination to PSO (red lines), SOP (blue lines) and SPO (green lines). Reactions on the surfaces of doublet and quartet spin multiplicity are shown as solid and dashed lines, respectively.

Interestingly, although ^2SPO is the most stable of the recombination products, very little of this species forms because the exit channel from ^2SPO to PO + S is 70 kJ mol^{-1} below the reactant entrance channel, indicating that collisional stabilization is very unlikely even at 1000 bar. ^4SPO is difficult to access because of the barrier of 44 kJ mol^{-1} above the entrance channel, but even if the barrier were crossed, the exit channel to PO + S is 70 kJ mol^{-1} below the entrance channel.

4. Conclusion

The $\text{P} + \text{SO} \rightarrow \text{PO} + \text{S}$ reaction is a fundamental reaction that can help explain why PO and not phosphorus is a fundamental marker of life on temperate exoplanets. There are no studies

in the literature that have examined the reaction. The present contribution is a first step in understanding the formation of PO molecules from the reaction between atomic phosphorus and sulfur monoxide. Our calculations show that the $\text{P} + \text{SO} \rightarrow \text{PO} + \text{S}$ reaction is exothermic. At pressures relevant for astrochemistry, the reaction is overwhelmingly bimolecular, with a predicted rate coefficient of $2.1 \times 10^{-10} (T/300)^{-0.23} \text{ cm}^3 \text{ molecule}^{-1} \text{ s}^{-1}$. This study opens the doors to quantify the importance of this reaction on the formation of PO relative to other formation pathways, such as the reaction of phosphorus with NO, i.e., $\text{P} + \text{NO} \rightarrow \text{PO} + \text{N}$. Finally, the intermediates in the $\text{P} + \text{SO} \rightarrow \text{PO} + \text{S}$ reaction are spectroscopically characterized to aid their detection in the laboratory or the ISM.

References

- Agúndez, M., Cernicharo, J., Decin, L., Encrenaz, P., & Teysier, D. 2014, *Astrophys J Lett*, 790 (IOP Publishing), L27
- Agúndez, M., Cernicharo, J., & Guélin, M. 2007, *Astrophys J Lett*, 662 (IOP Publishing), L91
- Altwegg, K., Balsiger, H., Bar-Nun, A., et al. 2016, *Sci Adv*, 2 (American Association for the Advancement of Science), e1600285
- De Beck, E., Kamiński, T., Patel, N. A., et al. 2013, *Astron Astrophys*, 558 (EDP Sciences), A132
- Dunning Jr, T. H. 1989, *J Chem Phys*, 90 (American Institute of Physics), 1007
- Dunning Jr, T. H., Peterson, K. A., & Wilson, A. K. 2001, *J Chem Phys*, 114 (American Institute of Physics), 9244
- Georgievskii, Y., & Klippenstein, S. J. 2005, *J Chem Phys*, 122 (American Institute of Physics), 194103
- Gilbert, R. G., & Smith, S. C. 1990 (Blackwell Scientific Publications Oxford)
- Głowacki, D. R., Liang, C.-H., Morley, C., Pilling, M. J., & Robertson, S. H. 2012, *J Phys Chem A*, 116 (ACS Publications), 9545
- Gobrecht, D., Cherchneff, I., Sarangi, A., Plane, J. M. C., & Bromley, S. T. 2016, *Astron Astrophys*, 585 (EDP Sciences), A6
- Gómez Martín, J. C., Brooke, J. S. A., Feng, W., et al. 2017, *J Geophys Res Atmos*, 122 (Wiley Online Library), 7678
- Griffith, E. J., Ponnampertuma, C., & Gabel, N. W. 1977, *Orig Life*, 8, 71, <https://doi.org/10.1007/BF00927976>
- Gulick, A. 1957, *Ann N Y Acad Sci*, 69 (Wiley Online Library), 309
- Halfen, D. T., Clouthier, D. J., & Ziurys, L. M. 2008, *Astrophys J*, 677
- Jiménez-Serra, I., Viti, S., Quénard, D., & Holdship, J. 2018, *Astrophys J*, 862 (IOP Publishing), 128
- Jorge, F. E., Canal Neto, A., Camiletti, G. G., & Machado, S. F. 2009, *J Chem Phys*, 130 (American Institute of Physics), 64108
- Knizia, G., Adler, T. B., & Werner, H.-J. 2009, *J Chem Phys*,

- 130 (American Institute of Physics), 54104
- Knowles, P. J., Hampel, C., & Werner, H.-J. 2000, *J Chem Phys*, 112 (American Institute of Physics), 3106
- Knowles, P. J., Hampel, C., & Werner, H. 1993, *J Chem Phys*, 99 (American Institute of Physics), 5219
- Knowles, P. J., & Werner, H.-J. 1985, *Chem Phys Lett*, 115 (Elsevier), 259
- Knowles, P. J., & Werner, H.-J. 1988, *Chem Phys Lett*, 145 (North-Holland), 514
- Lefloch, B., Vastel, C., Viti, S., et al. 2016, *Mon Not R Astron Soc*, 462 (The Royal Astronomical Society), 3937
- Lopez, X., Ugalde, J. M., Barrientos, C., Largo, A., & Redondo, P. 1993, *J Phys Chem*, 97 (ACS Publications), 1521
- Maciá, E., Hernández, M. V., & Oró, J. 1997, *Orig Life Evol Biosph*, 27 (Springer), 459
- Milam, S. N., Halfen, D. T., Tenenbaum, E. D., et al. 2008, *Astrophys J*, 684 (IOP Publishing), 618
- Namai, M., Sasaki, T., Ishikawa, H., Morikuni, H., & Mikami, N. 2009, *J Phys Chem A*, 113 (ACS Publications), 13081
- Peterson, K. A., Adler, T. B., & Werner, H.-J. 2008, *J Chem Phys*, 128 (American Institute of Physics), 84102
- Rivilla, V. M., Fontani, F., Beltrán, M. T., et al. 2016, *Astrophys J*, 826 (IOP Publishing), 161
- Senekowitsch, J. 1988 (University of Frankfurt Germany)
- Szalay, P. G., & Bartlett, R. J. 1993, *Chem Phys Lett*, 214 (North-Holland), 481
- Tenenbaum, E. D., Woolf, N. J., & Ziurys, L. M. 2007, *Astrophys J Lett*, 666 (IOP Publishing), L29
- Trabelsi, T., Al Mogren, M. M., Hochlaf, M., & Francisco, J. S. 2018, *J Chem Phys*, 148
- Turner, B. E., & Bally, J. 1987, *Astrophys J*, 321, L75
- Werner, H., & Knowles, P. J. 1985, *J Chem Phys*, 82 (American Institute of Physics), 5053
- Werner, H., & Knowles, P. J. 1988, *J Chem Phys*, 89 (American Institute of Physics), 5803
- Wilson, A. K., van Mourik, T., & Dunning Jr, T. H. 1996, *J Mol Struct THEOCHEM*, 388 (Elsevier), 339
- Yamaguchi, T., Takano, S., Sakai, N., et al. 2011, *Publ Astron Soc Japan*, 63 (Oxford University Press Oxford, UK), L37